DOI: 10.1049/mna2.12012

The Institution of Engineering and Technology WILEY

LETTER

In situ synthesis of metal-free N-GQD@g-C_3N_4 photocatalyst for enhancing photocatalytic activity

1 | INTRODUCTION

g-C_3N_4 as photocatalysts has attracted lots of attention due to metal-free, non-toxic, low-cost and stability for applications in water splitting, reduction of CO_2, removal of organic materials, chemical synthesis and so on [1–5]. However, single g-C_3N_4 exhibited low photocatalytic activity due to low separation efficiency of electron-hole, restricting its real applications [6]. Recently, co-catalysts were used to tune band structures, improving separation efficiency of electron–hole [7–15], such as noble metal (e.g. Au, Ag and Pt), inorganic semiconductor (e.g. TiO_2, ZnO, $GdVO_4$), C-based material (carbon nanotubes, graphene oxides and graphene quantum dots). Among these co-catalysts, the graphene quantum dots (GQDs) were most promising co-catalysts due to metal-free, unique photo-induced electron transfer, photo-luminescence and electron reservoir properties [15]. Therefore, there were some works reporting the preparation and photocatalytic performance of GQDs/g-C_3N_4 photocatalytic systems [15–23]. For example, GQDs/g-C_3N_4 nanorods were prepared by mixing method. The GQDs and g-C_3N_4 were firstly prepared, respectively, and then were mixed in water to form GQDs/g-C_3N_4. The removal efficiency was about 80.0% for photocatalytic degradation of oxytetracycline aqueous solution (15.0 mg/L) after 120 min [15]. S, N-GQDs/g-C_3N_4 was prepared by the similar mixing method. The removal efficiency was about 76.0% for photocatalytic degradation of RhB aqueous solution (5.0 mg/L) after 90.0 min [16]. GQDs/mpg-C_3N_4 was prepared by the similar mixing method. The removal efficiency was about 98.0% for photocatalytic degradation of RhB aqueous solution (10.0 mg/L) after 120.0 min [17]. GQDs/g-C_3N_4 ultrathin nanosheets were prepared by the similar mixing method. The removal efficiency was about 98.0% for photocatalytic degradation of RhB aqueous solution (1.0 mg/L) after 60.0 min [21]. These works have confirmed that the photodegradation performance of g-C_3N_4 could be effectively improved. However, these GQDs/g-C_3N_4 were generally prepared by the mixing method, in which the GQDs were not uniformly modified on surface of g-C_3N_4 due to poor stability of g-C_3N_4 aggregate in water. It was not only difficult to precise control micro-structure of GQDs/g-C_3N_4, but also led to a decrease of photocatalytic activity. These problems restricted the real applications of GQDs/g-C_3N_4 in industry. To this end, a facile production of GQDs/g-C_3N_4 with good photodegradation performance has become one of the key issues.

Herein, a new N-GQD/g-C_3N_4 was prepared by an in situ method. The N-GQDs could be uniformly modified on surface of g-C_3N_4. Furthermore, the photodegradation performance of in situ synthesis N-GQDs/g-C_3N_4 was evaluated and compared with N-GQDs/g-C_3N_4 prepared by traditional mixing method. The study provided a simple synthesis method of g-C_3N_4 uniformly modified with N-GQDs for various applications.

2 | EXPERIMENT

2.1 | In situ synthesis of N-GQDs/g-C_3N_4

N-GQDs/g-C_3N_4 was prepared by the two-step process. Firstly, N-GQDs were synthesized according to the work [24]. 0.23 g citric acid and 0.6 g urea were dissolved in 12.0 mL water under stirring. The above mixing solution was transferred into a 50.0 mL Teflon-sealed autoclave and reacted at 160.0 °C for 8.0 h. Finally, the products were collected by centrifugation method to remove other impurities and then dispersed into water. Secondly, 10.0 g urea was put into 5.0 mL N-GQDs solution (2.0 mg/mL). The mixture was reacted at 500.0 °C for 3 h in a muffle furnace. After cooling to room temperature around 25.0 °C the powders were washed with water for three times, collected by filtration and finally dried at room temperature, forming in situ synthesis N-GQDs/g-C_3N_4. In addition, pure g-C_3N_4 and N-GQDs were prepared according to above similar process. A specified volume of N-GQD solution was mixed with g-C_3N_4 under vigorously stirring. The products were collected by centrifugation and washed for three times with deionized water, forming mixing synthesis N-GQDs/g-C_3N_4.

2.2 | Characterizations

Crystal structure of samples was characterized by an X-ray diffractometer (HAOYUAN) using Cu Kα (λ = 0.1546 nm).

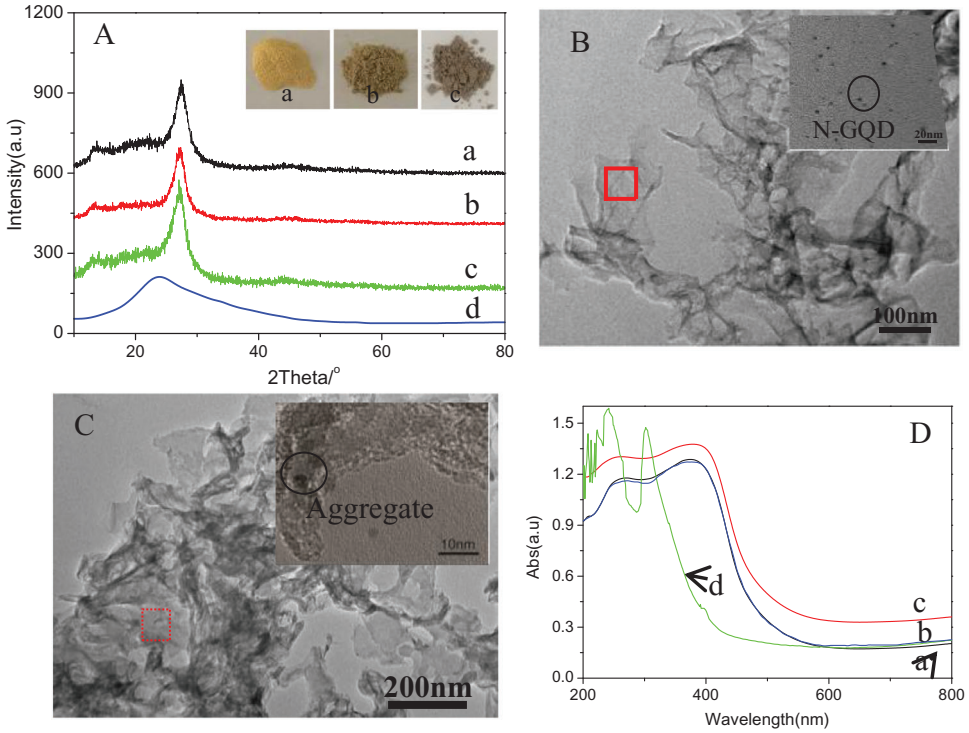

FIGURE 1 (A) XRD patterns of (a) g-C_3N_4, (b) mixing and (c) in situ synthesis N-GQDs/g-C_3N_4, (d) N-GQDs. TEM image of (B) in situ and (C) mixing synthesis N-GQDs/g-C_3N_4. (D) UV-DRS of (a) g-C_3N_4, (b) mixing and (c) in situ synthesis N-GQDs/g-C_3N_4, (d) N-GQDs. The insets of (A) are the optical photographs of (a) g-C_3N_4, (b) mixing and (c) in situ synthesis N-GQDs/g-C_3N_4. The inset of (B) and (C) is magnified TEM image of the N-GQDs/g-C_3N_4 region of marked in red

The morphology and size of samples were characterized by transmission electron microscopy (TEM, JEM-2010); UV absorption property was carried out on a UV–vis spectrophotometer. The fluorescence of sample was obtained on a fluoroscopic photometer (DF 2000). The specific surface area was measured by the BET method by nitrogen adsorption–desorption isotherms at 77.0 K. The photodegradation performance of samples was evaluated as shown in following. 50.0 mg N-GQDs/g-C_3N_4 was dispersed in 50.0 mL RhB solution (15.0 mg/L) under magnetically stirring in the dark for 1.0 h. The above mixture was irradiation under a 500.0 W halogen lamp ($\lambda > 400$ nm) for various time. At certain time intervals, 4.0 mL suspension solution was taken out and the photocatalyst was removed by centrifugation method. Then, the supernatant solution was characterized by UV–vis.

3 | RESULTS AND DISCUSSION

Figure 1(A) shows a weak diffraction peak at ca. 23.0°, corresponding to amorphous N-GQDs [25]. Other curves all showed two strong peaks at 13.1° and 27.5°, which were assigned to the (100) and (002) planes of g-C_3N_4, respectively (JCPDS card No. 87-1526) [17]. The diffraction peak of N-GQDs was not observed due to that the broad and weak peak of N-GQDs at 23.0° overlapped with the peak of g-C_3N_4 [16]. The pure g-C_3N_4 was dark yellow colour as shown in inset of Figure 1(A). In contrast, the N-GQDs/g-C_3N_4 showed uniformly light yellow and gray. The change of colour was attributed to change in energy structure of g-C_3N_4 due to introduce N-GQDs [26]. These results confirmed the formation of N-GQDs/g-C_3N_4. Figure 1(B) shows the TEM image of N-GQDs/g-C_3N_4. It clearly showed some nanosheets, which were assigned to g-C_3N_4. Furthermore, there were some dots on surface of nanosheet as shown in inset of Figure 1(B). Although the N-GQDs/g-C_3N_4 prepared by the mixing method also showed similar nanosheet structure (Figure 1(C)), yet, lot of aggregated dots were observed on surface of nanosheet as shown in inset of Figure 1(C). These results confirmed that the N-GQDs were uniformly modified on surface of g-C_3N_4 nanosheet by in situ synthesis [24]. Figure 1(D) shows UV–vis absorption spectra of N-GQDs, g-C_3N_4 and N-GQDs/g-C_3N_4. The single N-GQDs showed a UV absorption from 200.0 to 400.0 nm. In a comparison, single g-C_3N_4 clearly showed a UV–vis absorption from 200.0 to 550.0 nm. Especially was found that in situ synthesis N-GQDs/g-C_3N_4 clearly showed a distinct enhanced absorption from 200.0 to 800.0 nm comparing with single g-C_3N_4 and mixing synthesis N-GQDs/g-C_3N_4. These results indicated good UV–vis absorption ability of in situ synthesis N-GQDs/g-C_3N_4.

Fluorescent spectra of single g-C_3N_4 and N-GQDs/g-C_3N_4 were characterized and compared as shown in Figure 2(A). A similar emission peak of ca. 412.0 nm was observed for all samples, which was attributed to the recombination of the excited

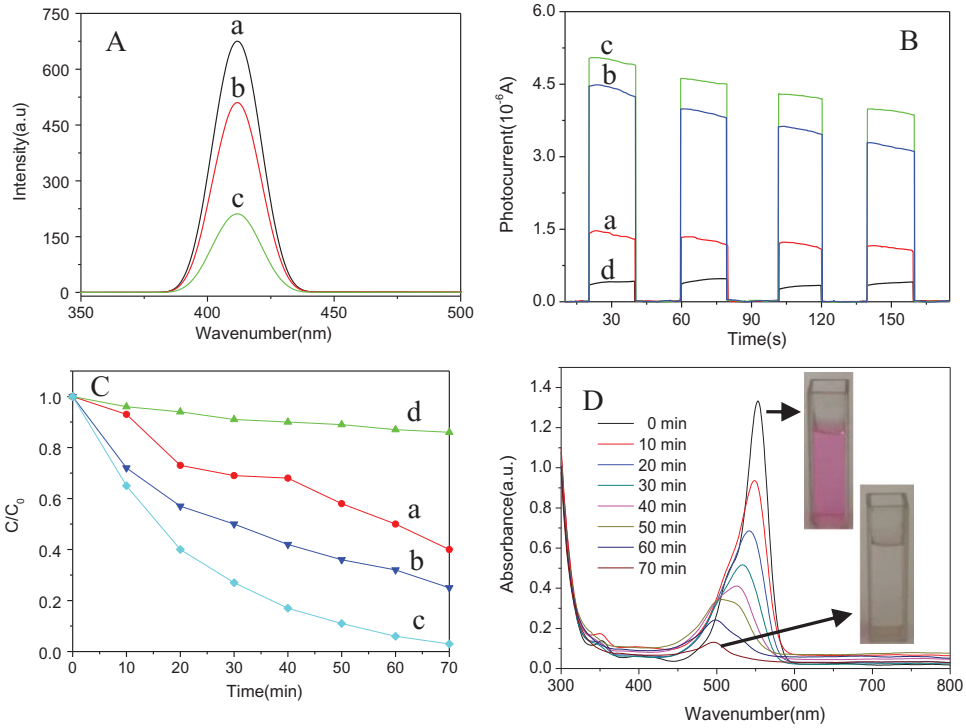

FIGURE 2 (A) PL spectra of (a) g-C_3N_4, (b) mixing and (c) in situ synthesis N-GQDs/g-C_3N_4 under an excitation wavelength of 390.0 nm. (B) Transient photocurrent curves of (a) N-GQD, (b) g-C_3N_4, (c) mixing and (d) in situ synthesis N-GQDs/g-C_3N_4 under 610–750 nm light irradiation. (C) Photodegradation of RhB with different photocatalysts of (a) pure N-GQD, (b) g-C_3N_4, (c) mixing and (d) in situ synthesis N-GQDs/g-C_3N_4 under visible light irradiation. (D) UV–vis spectra of RhB solution as function of natural outdoor light irradiation time in presence of in situ synthesis N-GQDs/g-C_3N_4. The insets of (D) are the optical photographs of RhB solution before and after natural outdoor light irradiation

electron–hole pairs of g-C_3N_4 [24, 27]. In addition, the emission peak intensity of N-GQDs/g-C_3N_4 was obviously lower than that of single g-C_3N_4. The result indicated that the N-GQDs could effectively suppress recombination of excited electron–hole pairs of g-C_3N_4 [26]. The emission peak intensity of in situ synthesis N-GQDs/g-C_3N_4 was lower than that of mixing synthesis N-GQDs/g-C_3N_4. The result suggested that the recombination of excited electron–hole pairs also strongly depended on distribution of N-GQDs on surface of g-C_3N_4. Figure 2(B) shows the photocurrent of various samples under visible light irradiation. Generally, a larger photocurrent indicated a longer lifetime and larger separation efficiency of photogenerated carriers [28]. The photocurrent intensity of in situ synthesis N-GQDs/g-C_3N_4 was obviously larger than that of single g-C_3N_4, N-GQDs or mixing synthesis N-GQDs/g-C_3N_4. The result confirmed that the uniform distribution of N-GQDs on surface of g-C_3N_4 could also effectively improve separation efficiency of the charge carriers. Figure 2(C) shows photodegradation performance of various samples. After 70.0 min irradiation, the concentration of RhB was few changes, indicating a poor photodegradation performance of N-GQDs under visible light [29]. Under the same condition, the removal efficiency of RhB was about 55.0% for single g-C_3N_4. As expected, when N-GQDs were combined with g-C_3N_4, the removal efficiency was obviously enhanced to 99.8% and 75.0% for the in situ and mixing synthesis N-GQDs/g-C_3N_4, respectively. The photodegradation performance of in situ synthesis N-GQDs/g-C_3N_4 was further evaluated under sun light irradiation as shown in Figure 2(D). The UV–vis absorption peak of RhB solution decreased with increase in irradiation time and almost completely disappeared after 70.0 min. The purple solution changed to colourless solution after 70.0 min. The result indicated that the RhB was photodegraded under sun light irradiation by N-GQDs/g-C_3N_4.

Here, the specific degradation rate (SDR, mg/g·min) was proposed to compare photodegradation performance of different photocatalysts under irradiation with same radiant power density [30].

$$\mathrm{SDR} = \frac{V \times (C_0 - C_t)}{M \times T}$$

where, V is volume of RhB solution (L). C_0 (mg/L) and C_t (mg/L) are the concentration of RhB solution before and after photodegradation, respectively. M (g) and T (min) are the mass of N-GQDs/g-C_3N_4 and irradiation time, respectively. By comparing with SDR of present N-GQDs/g-C_3N_4 and others photocatalysts based on g-C_3N_4 [10–12, 16, 17, 28, 31, 32] (Table 1), present N-GQDs/g-C_3N_4 had largest SDR, indicating a best photodegradation performance. Generally, the photodegradation performance strongly depended on special surface area, band gap, optical absorption ability, separation efficiency of the charge carriers and recombination of the excited electron–hole pairs [30].The special surface area of g-C_3N_4

TABLE 1 The photocatalytic activity and structure of photocatalysts based on g-C_3N_4

Sample	SDR (mg/g·min)	*Eg* (eV)	Surface area (m^2/g)	Ref.
In situ synthesis N-GQDs/g-C_3N_4	0.22	2.61	16.5	Present
Mixing synthesis N-GQDs/g-C_3N_4	0.16	2.69	15.4	
S,N-GQDs/g-C_3N_4	0.11	—	45.6	[16]
GQDs/mpg-C_3N_4	0.15	—	71.3	[17]
ZnO/g-C_3N_4	0.033	—	13.2	[11]
$GdVO_4$/g-C_3N_4	0.083	2.36	37.0	[10]
Fe_2O_3/g-C_3N_4	0.0375	2.5	—	[31]
Bi_2S_3/g-C_3N_4	0.08	2.25	—	[32]
TiO_2/g-C_3N_4	0.2	—	—	[12]
Ag_2O/g-C_3N_4	0.125	2.13	—	[28]

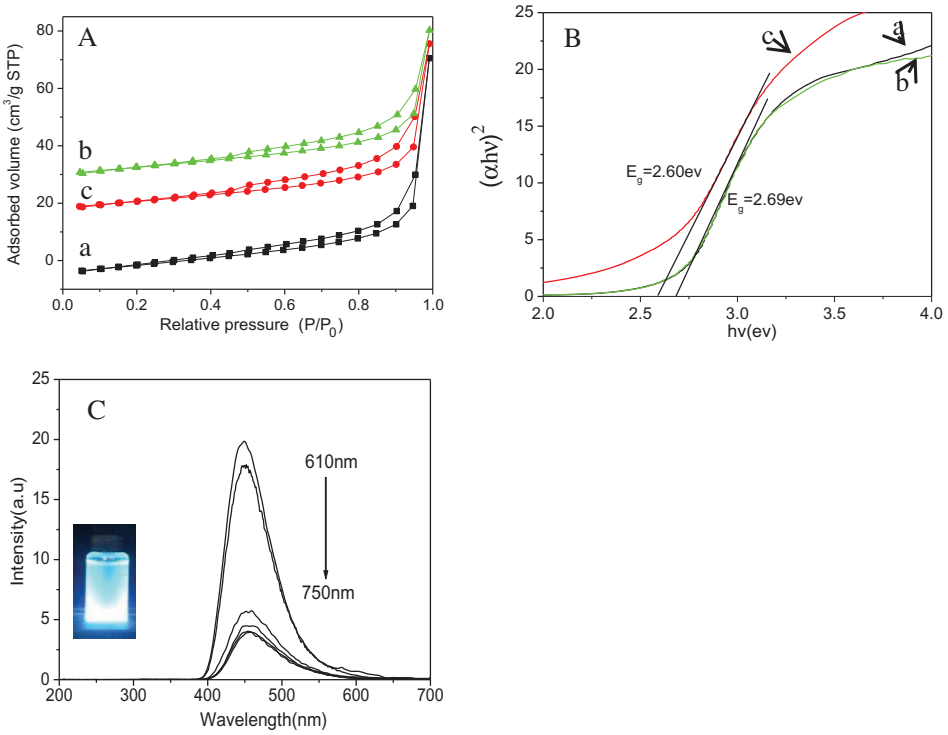

FIGURE 3 (A) Nitrogen adsorption–desorption isotherm curve of (a) g-C_3N_4, (b) mixing and (c) in situ synthesis N-GQDs/g-C_3N_4. (B) $(Ah\upsilon)^{1/2}$ versus $h\upsilon$ curve of (a) g-C_3N_4, (b) mixing and (c) in situ synthesis N-GQDs/g-C_3N_4. (C) PL spectra of N-GQDs under various excitation wavelengths of 610–750 nm, the inset of (C) is the optical photograph of N-GQDs solution under 365.0 nm and visible light

and N-GQDs/g-C_3N_4 was characterized and compared by N_2 adsorption–desorption isotherm as shown in Figure 3(A). It was about 19.6, 16.5 and 15.4 m^2/g for single g-C_3N_4, in situ synthesis N-GQDs/g-C_3N and mixing synthesis N-GQDs/g-C_3N_4, respectively. The optical band gap (*Eg*) of g-C_3N_4 and N-GQDs/g-C_3N_4 was estimated from the intercept of the tangents to the plots of $(Ah\upsilon)^{1/2}$ versus photo energy plots as shown in Figure 3(B). The *Eg* value of mixing synthesis N-GQDs/g-C_3N_4 was about 2.69 eV, which was similar with theoretical value of g-C_3N_4 [33]. In comparison, the *Eg* of in situ synthesis N-GQDs/g-C_3N_4 was reduced to 2.6 eV. The photoluminescence (PL) of N-GQDs was characterized by using different excitation wavelengths as shown in Figure 3(C). When excited by red light (λ = 610–750 nm), the N-GQDs showed a photoluminescence with short wavelength (400–500 nm), which could be absorbed by the g-C_3N_4. The upconversion property of N-GQDs could enhance the visible-light utilization [24]. Based on above experimental results, the good photodegradation performance mainly attributed to better separation efficiency of the charge carriers, fewer recombination of excited electron–hole pairs and better optical absorption ability, resulting from uniform distribution of N-GQDs on

surface of g-C_3N_4. At the same reason, although in situ synthesis N-GQDs/g-C_3N showed lower specific surface area, it still exhibited higher photocatalytic activity comparing with other GQDs/g-C_3N_4 reported in previous works [16, 17]. These results indicate that the uniform distribution of co-catalysts on surface of photocatalysts is also the key role for improving photodegradation performance of photocatalysts.

4 | CONCLUSION

In summary, N-GQDs/g-C_3N_4 were prepared by the in situ synthesis method. It was found that the N-GQDs could be uniform distribution on surface of g-C_3N_4. Furthermore, the N-GQDs/g-C_3N_4 possessed good photodegradation performance toward RhB under visible light irradiation. The result was attributed to more electron transfer between g-C_3N_4 and N-GQD, resulting from uniform distribution of N-GQDs on surface of g-C_3N_4. This study provides a new method to develop g-C_3N_4-based photocatalysts with high performance.

ACKNOWLEDGMENTS

This work was supported by the Shanxi Provincial Natural Science Foundation of China (201801D121104).

Yang Cao[1]
Luyang Sheng[1]
He Cheng[1]
Congxue Wang[1]
Youyi Sun[1]
Qiang Fu[2]

[1] *School of Materials Science and Technology, North University of China, Taiyuan 030051, People's Republic of China*
[2] *School of Civil and Environmental Engineering, University of Technology Sydney, Ultimo, New South Wales 2007, Australia*

Correspondence
Youyi Sun, School of Materials Science and Technology, North University of China, Taiyuan 030051, People's Republic of China.
Email: syyi@mail.ustc.edu.cn

REFERENCES

1. Li, K., et al.: Modification of g-C_3N_4 nanosheets by carbon quantum dots for highly efficient photocatalytic generation of hydrogen. Appl. Surf. Sci. 375, 110–117 (2016)
2. Ye, L.Q., et al.: Phosphorylation of g-C_3N_4 for enhanced photocatalytic CO_2 reduction. Chem. Eng. J. 304, 376–383 (2016)
3. Qu, L.L., et al.: Recyclable visible light-driven O-g-C_3N_4/Graphene Oxide/N-Carbon nanotube membrane for efficient removal of organic pollutants. ACS Appl. Mater. Interfaces 10, 42427–42435 (2018)
4. Deng, J., et al.: Enhanced visible-light-driven photocatalytic bacteria disinfection by g-C_3N_4-AgBr. Colloids Surf., B 152, 49–57 (2017)
5. Zhang, L.Q., et al.: Highly active TiO_2/g-C_3N_4/G photocatalyst with extended spectral response towards selective reduction of nitrobenzene. Appl. Catal., B 203, 1–8 (2017)
6. Zhang, S., et al.: Recent developments in fabrication and structure regulation of visible-light riven g-C_3N_4-based photocatalysts towards water purification: A critical Review. Catal. Today 335, 65–77 (2019)
7. Qin, J.Y., et al.: Improving the photocatalytic hydrogen production of Ag/g-C_3N_4 nanocomposites by dye-sensitization under visible light irradiation. Nanoscale 8, 2249–2259 (2016)
8. Liu, M.J., et al.: Enhanced photocatalytic H_2-production activity of g-C_3N_4 nanosheets via optimal photodeposition of Pt as cocatalyst. ACS Sustainable Chem. Eng. 6, 10472–10480 (2018)
9. Li, H., et al.: Enhanced selective photocatalytic reduction of CO_2 to CH_4 over plasmonic Au modified g-C_3N_4 photocatalyst under UV-vis light irradiation. Appl. Surf. Sci. 439, 552–559 (2018)
10. He, Y.M., et al.: Efficient degradation of RhB over $GdVO_4$/g-C_3N_4 composites under visible-light Irradiation. Chem. Eng. J. 215-216, 721–730 (2013)
11. Liu, W., et al.: Significantly enhanced visible-light photocatalytic activity of g-C_3N_4 via ZnO modification and the mechanism study. J. Mol. Catal. A: Chem. 368-369, 9–15 (2013)
12. Tong, Z.W., et al.: Biomimetic fabrication of g-C_3N_4/TiO_2 nanosheets with enhanced photocatalytic activity toward organic pollutant degradation. Chem. Eng. J. 260, 117–125 (2015)
13. Wang, G.Q., et al.: Graphitic carbon nitride/multiwalled carbon nanotubes composite as Pt-free counter electrode for high-efficiency dye-sensitized solar cells. Electrochim. Acta 187, 243–248 (2016)
14. Wang, N.N., et al.: A g-C_3N_4 supported graphene oxide/$AgPO_4$ composite with remarkably enhanced photocatalytic activity under visible light. Catal. Commun. 73, 74–79 (2016)
15. Yuan, A.L., et al.: Graphene quantum dots decorated graphitic carbon nitride nanorods for photocatalytic removal of antibiotics. J. Colloid Interface Sci. 548, 56–65 (2019)
16. Cai, A., et al.: Graphitic carbon nitride decorated with S, N co-doped graphene quantum dots for enhanced visible-light-driven photocatalysis. J. Alloys Compd. 692, 183–189 (2017)
17. Liu, J., et al.: Graphene quantum dots modified mesoporous graphite carbon nitride with significant enhancement of photocatalytic activity. Appl. Catal., B 207, 429–437 (2017)
18. Xu, C.Y., et al.: Sulfur doped graphitic carbon nitride decorated with graphene quantum dots for efficient metal-free electrocatalyst. J. Mater. Chem. A 3, 1841–1846 (2015)
19. Ma, Z.J., et al.: Interfacial electronic structure and charge transfer of hybrid graphene quantum dot and graphitic carbon nitride nanocomposites: Insights into high efficiency for photocatalytic solar water splitting. Phys. Chem. Chem. Phys. 18, 1050–1058 (2016)
20. Wang, R.L., et al.: Graphene quantum dot modifified g-C_3N_4 for enhanced photocatalytic oxidation of ammonia performance. RSC Adv. 7, 51687–51694 (2017)
21. Qian, J.J., et al.: Graphene quantum dots-assisted exfoliation of graphitic carbon nitride to prepare metal-free zero-dimensional/two-dimensional composite photocatalysts. J. Mater. Sci. 53, 12103–12114 (2018)
22. Zou, J.P., et al.: Synthesis and efficient visible light photocatalytic H_2 evolution of a metal-free g-C_3N_4/graphene quantum dots hybrid photocatalyst. Appl. Catal., B 193, 103–109 (2016)
23. Mou, Z.G., et al.: Chemical interaction in nitrogen-doped graphene quantum dots/graphitic carbon nitride heterostructures with enhanced photocatalytic H_2 evolution. Energy Technol. 7, 1800589 (2019)
24. Sun, Y.Y., et al.: Facile synthesis of free-metal ternary composites for ultrafast photocatalytic degradation of organic pollutant. Catal. Today 340, 294–301 (2020)
25. Hu, C.F., et al.: One-step preparation of nitrogen-doped graphene quantum dots from oxidized debris of graphene oxide. J. Mater. Chem. B 1, 39–42 (2013)
26. Wang, C.X., et al.: Facile synthesis of nanoporpous graphitic carbon nitride photocatalyst coupled with N-doped graphene quantum dots for efficient photo-degradation dyes under nature solar light radiation. Diamond Relat. Mater. 89, 197–205 (2018)
27. Zhang, P., et al.: Design of Cu-Cu_2O/g-C_3N_4 nanocomponent photocatalysts for hydrogen evolution under visible light irradiation using water-soluble Erythrosin B dye sensitization. Appl. Surf. Sci. 391, 404–414 (2017)
28. Shi, L., et al.: Enhanced photocatalytic activity over the Ag_2O-g-C_3N_4 composite under visible light. Catal. Sci. Technol. 4, 758–765 (2014)

29. Chen, F., et al.: Highly selective deethylation of rhodamine B: Adsorption and photooxidation pathways of the dye on the TiO_2/SiO_2 composite photocatalyst. Int. J. Photoenergy 5, 209–217 (2003)
30. Sun, Y.Y., et al.: Facile synthesis of highly efficient photocatalysts based on organic small molecular co-catalyst. Appl. Surf. Sci. 469, 553–563 (2019)
31. Ye, S., et al.: Facile fabrication of magnetically separable graphitic carbon nitride photocatalysts with enhanced photocatalytic activity under visible light. J. Mater. Chem. A. 1, 3008–3015 (2013)
32. Rong, X.S., et al.: Coupling with a narrow-band-gap semiconductor for enhancement of visible-light photocatalytic activity: Preparation of $Bi_2S_3/g\text{-}C_3N_4$ and application for degradation of RhB. RSC Adv. 5, 24944–24952 (2015)
33. Li, Q., et al.: High efficiency photocatalysis for pollutant degradation with MoS2/g-C_3N_4 heterostructures. Langmuir 30, 8965–8972 (2014)